

---

# KOLMOGOROV-ARNOLD NETWORKS FOR TIME SERIES GRANGER CAUSALITY INFERENCE

---

Meiliang Liu, Yunfang Xu, Zijin Li, Zhengye Si, Xiaoxiao Yang, Xinyue Yang, Zhiwen Zhao  
School of Artificial intelligence  
Beijing Normal University  
Beijing

## ABSTRACT

We introduce Granger Causality Kolmogorov-Arnold Networks (GCKAN), an innovative architecture that extends the recently proposed Kolmogorov-Arnold Networks (KAN) to the domain of causal inference. By extracting base weights from KAN layers and incorporating the sparsity-inducing penalty along with ridge regularization, GCKAN infers the Granger causality from time series while enabling automatic time lag selection. Additionally, we propose an algorithm leveraging time-reversed Granger causality to enhance inference accuracy. The algorithm compares prediction and sparse-inducing losses derived from the original and time-reversed series, automatically selecting the casual relationship with the higher score or integrating the results to mitigate spurious connectivities. Comprehensive experiments conducted on Lorenz-96, gene regulatory networks, fMRI BOLD signals, and VAR datasets demonstrate that the proposed model achieves competitive performance to state-of-the-art methods in inferring Granger causality from nonlinear, high-dimensional, and limited-sample time series.

**Keywords** Granger causality · Time series · Kolmogorov-Arnold Networks

## 1 Introduction

Granger causality is a statistical framework for analyzing the causality between time series. It offers a powerful tool to investigate temporal dependencies and infer the direction of influence between variables [Seth(2007), Maziarz(2015), Friston et al.(2014)Friston, Bastos, Oswal, van Wijk, Richter, and Litvak, Shojaie and Fox(2022)]. By examining the past values of a series, Granger causality seeks to determine if the historical knowledge of one variable improves the prediction of another [Bressler and Seth(2011), Barnett and Seth(2014)]. Revealing inner interactions from observational time series has made Granger causality useful for the investigation in many fields, such as econometrics [Mele et al.(2022)Mele, Magazzino, Schneider, Gurrieri, and Golpira], neuroscience [Chen et al.(2023)Chen, Ginoux, Carbo-Tano, Mora, Walczak, and Wyart], climate science [Ren et al.(2023)Ren, Li, He, and Lucey], etc.

Recently, there has been a growing interest in incorporating neural networks into the study of Granger causality due to their inherent nonlinear mapping capabilities. For now, a variety of neural Granger causality models have been proposed, mainly based on multi-layer perceptron (MLP) [Tank et al.(2022)Tank, Covert, Foti, Shojaie, and Fox, Bussmann et al.(2021)Bussmann, Nys, and Latré, Zhou et al.(2024)Zhou, Bai, Yu, Zhao, and Chen], recurrent neural network (RNN) [Khanna and Tan(2019), Tank et al.(2022)Tank, Covert, Foti, Shojaie, and Fox], convolutional neural network (CNN) [Nauta et al.(2019)Nauta, Bucur, and Seifert], or their combination [Cheng et al.(2024)Cheng, Li, Xiao, Li, Suo, He, and Dai]. These models have achieved significant improvements in inferring nonlinear Granger causality but still have certain limitations: (1) RNN-based models are more suitable for processing long time series, but experience decreased causal inference performance in the limited time-samples scenario. Additionally, these models have only an explicit dependence on one past timepoint, which makes them unable to select time lags automatically; (2) MLP-based models can automatically select time lags but face the challenge of low inference efficiency when dealing with high-dimensional and noisy time series. (3) CNN-based models have been shown to perform ineffectively on many nonlinear datasets.

Therefore, our motivation is to propose a neural network-based Granger causality model that can effectively infer causal relationships from high-dimensional nonlinear time series data with limited sampling points, and also can select time lags automatically. We consider a novel framework, the Kolmogorov-Arnold Network (KAN) [Liu et al.(2024)Liu, Wang, Vaidya, Ruehle, Halverson, Soljačić, Hou, and Tegmark], to construct a Granger causality inference model. Different from MLP, which uses learnable weights on the edges and fixed activation functions on the nodes, KAN uses learnable univariate functions at the edges and simple summation operations at the nodes, making its computational graph much smaller than that of MLP [Kiamari et al.(2024)Kiamari, Kiamari, and Krishnamachari, Hou and Zhang(2024)].

Our work extends the basic KAN to the field of causal inference and aims to evaluate whether the KAN-based model has the potential to outperform MLP-based and RNN-based baselines. Our main contributions are as follows:

- To our best knowledge, this is the first work to utilize KAN for multivariate Granger causality inference.
- We propose a simple but effective Granger causality model based on KAN. The model only needs to extract the base weight of the KAN layers and impose the sparsity-inducing penalty and ridge regularization to infer Granger causality.
- We propose an algorithm that automatically selects the Granger causality adjacency matrix with the higher inference performance from the origin or time-reversed time series or mitigates spurious connections by fusing both of them.
- Extensive experiments on Lorenz-96, Gene regulatory networks, fMRI BOLD, and VAR datasets validate that the proposed model attains stable and competitive performances in Granger causality inference.

## 2 Background and Related Works

### 2.1 Background: Neural network-based Granger causality

Recently, inferring Granger causality from nonlinear time series via neural networks has attracted widespread attention. [Tank et al.(2022)Tank, Covert, Foti, Shojaie, and Fox] proposed the cMLP and cLSTM, which extract the first-layer weights of multi-layer perceptron (MLP) and long short-term memory (LSTM), respectively, and impose the sparsity-inducing penalty to infer Granger causality. [Bussmann et al.(2021)Bussmann, Nys, and Latré] proposed the Neural Additive Vector Autoregression (NAVAR) model based on MLP and LSTM, called NAVAR(MLP) and NAVAR(LSTM), for Granger causality inference. [Khanna and Tan(2019)] proposed the economy-SRU (eSRU) model, which extracts weights from statistical recurrent units (SRU) and regularizes them to infer Granger causality. In addition, [Nauta et al.(2019)Nauta, Bucur, and Seifert] proposed a temporal causal discovery framework (TCDF) based on temporal convolutional network (TCN) and causal verification steps to infer Granger causality and select time lags. [Cheng et al.(2023)Cheng, Yang, Xiao, Li, Suo, He, and Dai] proposed Causal discovery from irregular Time-Series (CUTS), which can effectively infer Granger causality from data with random missing or non-uniform sampling frequency. Subsequently, to solve the problems of large causal graphs and redundant data prediction modules of CUTS, [Cheng et al.(2024)Cheng, Li, Xiao, Li, Suo, He, and Dai] proposed the CUTS+, which introduced a coarse-to-fine causal discovery mechanism and a message-passing graph neural network (MPGNN) to achieve more accurate causal reasoning. [Marcinkevičs and Vogt(2021)] proposed a generalised vector autoregression (GVAR) based on the self-explaining neural network model, which effectively inferred causal relationships and improved the interpretability of the model. [Zhou et al.(2024)Zhou, Bai, Yu, Zhao, and Chen] proposed a neural Granger causality model based on Jacobi regularization (JRNGC), which only needs to construct a single model for all variables to achieve causal inference.

### 2.2 Related Works

#### 2.2.1 Component-wise nonlinear autoregressive (NAR)

Assume a  $p$ -dimensional nonlinear time series  $x_t = [x_{<t1}, \dots, x_{<tp}]$ , where  $x_{<ti} = (\dots, x_{<(t-2)i}, x_{<(t-1)i})$ . In the nonlinear autoregressive (NAR) model, the  $t^{th}$  time point  $x_t$  can be denoted as a function  $g$  of its past time values:

$$x_t = g(x_{<t1}, \dots, x_{<tp}) + e^t \quad (1)$$

Furthermore, in the component-wise NAR model, it is assumed that the  $t^{th}$  time point of each time series  $x_{ti}$  may depend on different past-time lags from all the series:

$$x_{ti} = g_i(x_{<t1}, \dots, x_{<tp}) + e^{ti} \quad (2)$$

To infer Granger causality from the component-wise NAR model, sparsity-inducing penalty is applied:

$$\min_W \sum_{t=K}^T (x_{ti} - g_i(x_{<t1}, \dots, x_{<tp}))^2 + \lambda \sum_{j=1}^p \Theta(W_{:,j}) \quad (3)$$

where  $W$  is extracted from the neural network,  $\Theta$  is the sparsity-inducing penalty that penalizes the parameters in  $W$  to zero,  $\lambda$  is the hyperparameter that controls the strength of the penalty. In the NAR model, if there exists a time lag  $k$ ,  $W_{:,j}^k$  contains non-zero parameters, time series  $j$  Granger-causes to time series  $i$ .

### 2.2.2 Time reversed Granger causality

The time-reversed Granger causality was initially introduced by [Haufe et al.(2013)Haufe, Nikulin, Müller, and Nolte], which was used to reduce spurious connections caused by volume conduction effects in analyzing Electroencephalogram (EEG) signals [van den Broek et al.(1998)van den Broek, Reinders, Donderwinkel, and Peters, Nunez et al.(1997)Nunez, Srinivasan, Westdorp, Wijesinghe, Tucker, Silberstein, and Cadusch]. Subsequently, [Winkler et al.(2016)Winkler, Panknin, Bartz, Müller, and Haufe] demonstrated that, in finite-order autoregressive processes, causal relationships would reversed in time-reversed time series. Moreover, comparing the causal relationship inferred from the original data and the time-reversed data can enhance the robustness of causal inference against noise. However, the proof of [Winkler et al.(2016)Winkler, Panknin, Bartz, Müller, and Haufe] is mainly for the linear system. However, the findings of [Winkler et al.(2016)Winkler, Panknin, Bartz, Müller, and Haufe] primarily apply to linear systems. Recent research indicates that in nonlinear chaotic systems, causal relationships inferred from time-reversed time series generally align with those from the original data, with perfect causal relationship reversal occurring only under specific conditions [Košenek and Hlinka(2021)].

### 2.2.3 Kolmogorov–Arnold Networks (KAN)

[Liu et al.(2024)Liu, Wang, Vaidya, Ruehle, Halverson, Soljačić, Hou, and Tegmark] proposed KAN, which has garnered attention as a compelling alternative to the multilayer perceptron (MLP). The theoretical foundation of MLP is rooted in the universal approximation theorem, which demonstrates that neural networks can approximate any continuous function under appropriate conditions [Pinkus(1999)]. By contrast, KAN is grounded in the Kolmogorov–Arnold (KA) representation theorem, which states that any multivariate continuous function can be represented by the sum of a finite number of univariate functions [Schmidt-Hieber(2021)].

**Theorem 2.1** *Let  $f : [0, 1]^n \rightarrow \mathbb{R}$  be a continuous multivariate function. There exist continuous univariate functions  $\Phi_q$  and  $\phi_{q,p}$  such that:*

$$f(x_1, x_2, \dots, x_n) = \sum_{i=1}^{2n+1} \Phi_q \left( \sum_{j=1}^n \phi_{q,p}(x_p) \right)$$

where  $\Phi_i : \mathbb{R} \rightarrow \mathbb{R}$  and  $\phi_{q,p} : [0, 1] \rightarrow \mathbb{R}$  are continuous functions.

Although the KA representation theorem is elegant and general, its application in deep learning remained limited before the work of [Liu et al.(2024)Liu, Wang, Vaidya, Ruehle, Halverson, Soljačić, Hou, and Tegmark]. This limitation can be attributed to two primary factors: (1) the function  $\phi_{q,p}$  is typically non-smooth; (2) the theorem is constrained to construct shallow neural networks with two-layer nonlinear architectures with limited hidden layer size. [Liu et al.(2024)Liu, Wang, Vaidya, Ruehle, Halverson, Soljačić, Hou, and Tegmark] do not strictly constrain the neural network to fully adhere to Theorem 2.1, but instead extended the network to arbitrary width and depth to be used in deep learning. Due to this alternation, KAN and its variants have been extensively applied across various domains, including computer vision, natural language processing, and time series forecasting. In this study, we develop our Granger causality model based on the code of efficientKAN<sup>1</sup>.

## 3 Model Architecture

### 3.1 Component-wise KAN

To extract the influence from input to output, we model each component  $g_i$  using a separate KAN. Let  $g_i$  take the form of a KAN with  $L - 1$  layers, and  $h^l$  are denoted as the  $l^{th}$  hidden layer. The trainable parameter of KAN including  $W_{base}$ ,  $W_{spline}$  on each layer,  $W_{base} = \{W_b^0, W_b^1, \dots, W_b^{L-1}\}$  and  $W_{spline} = \{W_s^0, W_s^1, \dots, W_s^{L-1}\}$ . We separate

<sup>1</sup><https://github.com/Blealtan/efficient-kan>

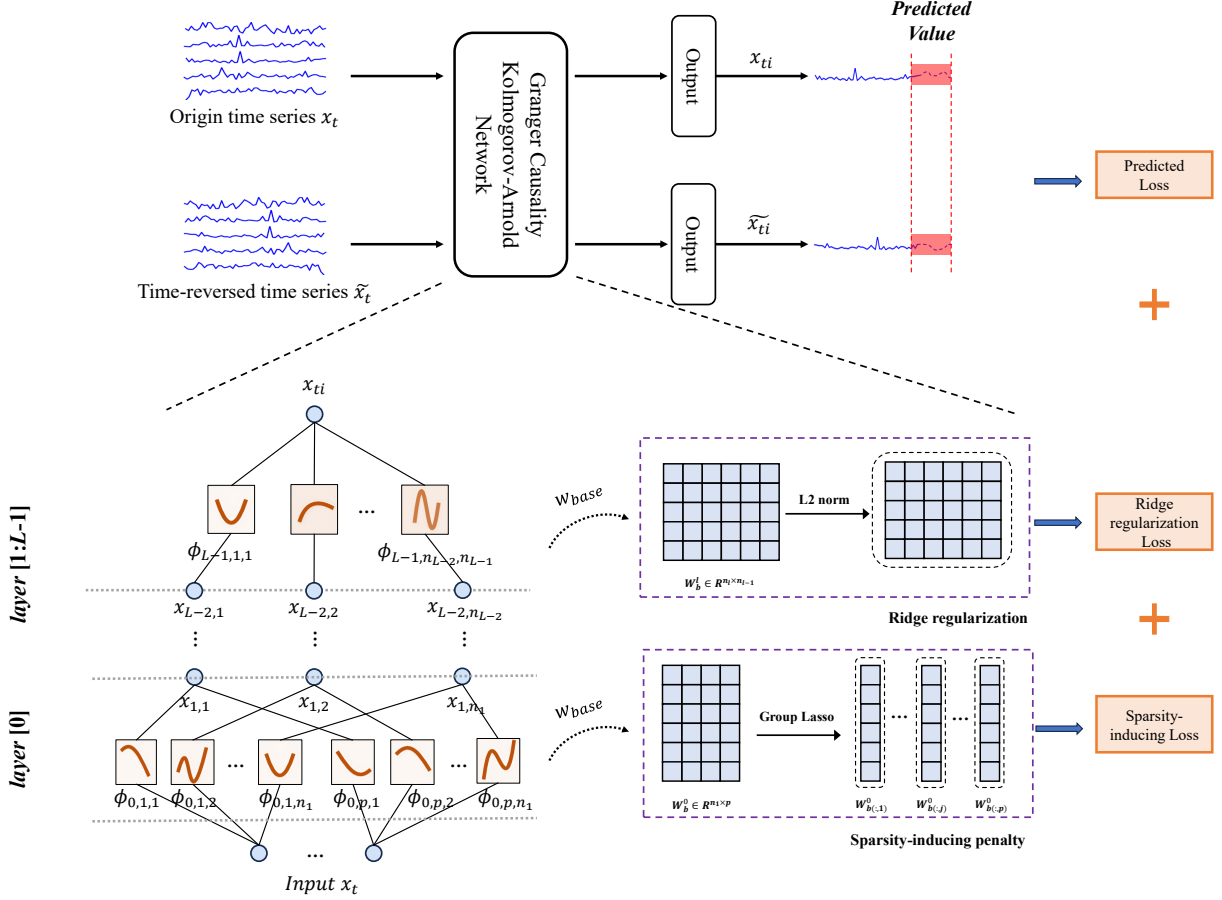


Figure 1: The architecture of GCKAN.

the  $W_{base}$  into the first layer weights  $W_b^0 \in \mathbb{R}^{H \times p}$ , and the other layers  $W_b^l \in \mathbb{R}^{H \times H}$  ( $0 < l < L$ ). By using these notations, the vector of the hidden units in the first layer  $h^1$  is denoted as:

$$\mathbf{h}^1 = \underbrace{\begin{pmatrix} \phi_{0,1,1}(\cdot) & \cdots & \phi_{0,1,n_0}(\cdot) \\ \phi_{0,2,1}(\cdot) & \cdots & \phi_{0,2,n_0}(\cdot) \\ \vdots & \vdots & \vdots \\ \phi_{0,n_1,1}(\cdot) & \cdots & \phi_{0,n_1,n_0}(\cdot) \end{pmatrix}}_{\Phi_0} \mathbf{x}_t \quad (4)$$

where  $n_0 = p$  is the input time series dimension,  $n_1$  is the first hidden layer size. Here, the  $\phi(x)$  is denoted as:

$$\phi(x) = W_b^0 b(x) + W_s^0 spline(x) \quad (5)$$

Subsequently, The vector of the hidden units in the layer  $l$  is denoted as:

$$\mathbf{h}^l = \underbrace{\begin{pmatrix} \phi_{l-1,1,1}(\cdot) & \cdots & \phi_{l-1,1,n_{l-1}}(\cdot) \\ \phi_{l-1,2,1}(\cdot) & \cdots & \phi_{l-1,2,n_{l-1}}(\cdot) \\ \vdots & \vdots & \vdots \\ \phi_{l-1,n_l,1}(\cdot) & \cdots & \phi_{l-1,n_l,n_{l-1}}(\cdot) \end{pmatrix}}_{\Phi_{l-1}} \mathbf{h}^{l-1} \quad (6)$$

where  $n_l$  and  $n_{l-1}$  is the  $l^{th}$  and  $l-1^{th}$  hidden layer size, respectively. Here, the  $\phi(x)$  is denoted as:

$$\phi(x) = W_b^l b(x) + W_s^l spline(x) \quad (7)$$

The time series  $x_t$  go through the  $L - 1$  hidden layers to generate the output  $x_{ti}$ , which is denoted as:

$$x_{ti} = g_i(x_t) + e_{ti} = \Phi_{L-1} \circ h^{L-1} + e_{ti} \quad (8)$$

where  $e_{ti}$  is the mean zero Gaussian noise.

### 3.2 Applying sparsity-inducing penalty and ridge regularization on KAN to infer Granger causality

According to Eq.3, the inference of Granger causality in Equation 8 uses component-wise NAR combined with sparsity-inducing penalty. In our study, we extract the base weight  $W_b^0$  of the first hidden layer and apply a group lasso penalty to the columns of the  $W_b^0$  matrices for each  $g_i$ , which is denoted as:

$$\text{GroupLasso}(W_{b^{(j)}}^0) = \left\| W_{b^{(j)}}^0 \right\|_F \quad (9)$$

where  $W_{b^{(j)}}^1$  is the  $j$  column of the  $W_b^1$  corresponding to the time series  $j$ .  $\|\cdot\|_F$  is denoted as the Frobenius matrix norm. The sparse-inducing loss  $\mathcal{L}_s$  is defined as:

$$\mathcal{L}_s = \lambda \sum_{j=1}^p \|W_{b^{(j)}}^0\|_F \quad (10)$$

$\lambda > 0$  is the group lasso hyperparameter that controls the penalty strength. For the base weight  $W_b^l$  of other hidden layers except the first hidden layer, we apply ridge regularization to them, which is denoted as:

$$\text{RidgeRegularization}(W_b^{1:L-1}) = \sum_{l=1}^{L-1} \|W_b^l\|_2 \quad (11)$$

where  $\|\cdot\|_2$  is denoted as the  $L2$  norm. The ridge regularization loss  $\mathcal{L}_r$  is defined as:

$$\mathcal{L}_r = \gamma \sum_{l=1}^{L-1} \|W_b^l\|_2 \quad (12)$$

$\gamma > 0$  is the ridge regularization hyperparameter that controls the regularization strength. Finally, the predicted loss is defined as:

$$\mathcal{L}_p = \sum_{i=1}^p (x_{ti} - g_i(x_t))^2 \quad (13)$$

Therefore, the loss function is defined as:

$$\mathcal{L} = \mathcal{L}_p + \mathcal{L}_s + \mathcal{L}_r \quad (14)$$

Since the proposed model is a component-wise architecture, a total of  $p$  models are needed to construct the complete Granger causality matrix. We extract the first hidden layer weight  $W_b^0$  to compute the  $i^{th}$  row of the Granger causality matrix  $G$ , which is denoted as:

$$G_{(i,:)} = \|W_{b^{(j)}}^0\|_F \quad (15)$$

### 3.3 Fusion of origin and time reversed time series

During the experiment, we observed that, in certain simulation trials, the causality scores derived from the original and reversed time series exhibit considerable divergence. Specifically, there were cases where the causality score from the original time series was higher, while in other cases, the reversed time series yielded a better score. Consequently, our objective is to develop an algorithm that can automatically select the matrix with the higher causality score from either the original or reversed time series or obtain more accurate inference results by fusing both of them.

Algorithm 1 summarizes the proposed procedure for fusing the original and reversed time series. In the Granger causality inference stage, a total of  $2p$  GCKAN models are required, with the first  $p$  models applied to the original time series and the next  $p$  models to the reversed time series (lines 3-4 in Algorithm 1). We use Equation (12) to calculate the Granger causality matrix of the original and reversed time series (line 5 in Algorithm 1). Subsequently, we compare the losses to determine whether to select a single matrix or fuse both matrices. Specifically, when the prediction loss and sparsity-induced loss of the original time series are both lower than those of the reversed time series, it suggests that the model's prediction and sparsity performance are superior for the original time series. Therefore, the Granger causality matrix derived from the original time series is chosen as the final matrix. Conversely, if the reversed time series exhibits

better performance, its corresponding Granger causality matrix is selected (lines 7-10 in Algorithm 1). In situations where the prediction loss and sparsity-inducing loss do not align between the two time series, we element-wise compare each element in the two matrices. If the absolute difference between the corresponding elements is below a predefined threshold (unified set to 0.05 in our study), the average of the two elements is taken. If the difference exceeds the threshold, the maximum value of the two elements is taken (lines 12-21 in Algorithm 1). In our experiments, this straightforward strategy can effectively improve the Granger causality inference performance of the proposed model.

---

**Algorithm 1** Fusion of origin and time reversed time series for inferring Granger causality with GCKAN

---

```

1: Input: The origin multivariate time series  $\{x_t\}$  with dimension  $p$ ; group lasso penalty hyperparameter  $\lambda$ ; ridge regularization hyperparameter  $\gamma$ ; threshold  $\theta$ 
2: Output: Estimate  $\hat{G}$  of the adjacency matrix of the GC graph.
3: Let  $\{\tilde{x}_t\}$  be the time-reversed time series of  $\{x_t\}$ ,  $\{x_1, x_2, \dots, x_T\} \equiv \{\tilde{x}_T, \tilde{x}_{T-1}, \dots, \tilde{x}_1\}$ .
4: Train  $2p$  GCKAN with hyperparameter  $\lambda$  and  $\gamma$  by minimizing losses in Equation 6 (first  $p$  models are trained on  $\{x_t\}$  and next  $p$  models are trained on  $\{\tilde{x}_t\}$ ).
5: Compute GC graph  $G$  and  $\tilde{G}$  from origin and time reversed time series using Equation 7.
6: Get predict loss  $\mathcal{L}_{p(o)}$ ,  $\mathcal{L}_{p(r)}$ , sparsity-inducing loss  $\mathcal{L}_{s(o)}$ ,  $\mathcal{L}_{s(r)}$  from origin and time reversed time series, respectively.
7: if  $\mathcal{L}_{p(o)} < \mathcal{L}_{p(r)}$  AND  $\mathcal{L}_{s(o)} < \mathcal{L}_{s(r)}$  then
8:    $\hat{G} = G$ 
9: else if  $\mathcal{L}_{p(o)} > \mathcal{L}_{p(r)}$  AND  $\mathcal{L}_{s(o)} > \mathcal{L}_{s(r)}$  then
10:   $\hat{G} = \tilde{G}$ 
11: else
12:   for  $i = 1$  to  $p$  do
13:     for  $j = 1$  to  $p$  do
14:       if  $abs(G_{i,j} - \tilde{G}_{i,j}) < \theta$  then
15:          $\hat{G}_{i,j} = \frac{1}{2}(G_{i,j} + \tilde{G}_{i,j})$ 
16:       else
17:          $\hat{G}_{i,j} = max(G_{i,j}, \tilde{G}_{i,j})$ 
18:       end if
19:     end for
20:   end for
21: end if
22: return  $\hat{G}$ .

```

---

## 4 Experiment

In this section, we show the performance of the proposed model (GCKAN) on four widely used benchmark datasets: Lorenz-96 model, fMRI BOLD signals, Gene regulatory networks, and VAR. Comparative experiments were conducted against several state-of-the-art models, including cMLP & cLSTM [Tank et al.(2022)Tank, Covert, Foti, Shojaie, and Fox], TCDF [Nauta et al.(2019)Nauta, Bucur, and Seifert], e-SRU [Khanna and Tan(2019)], GVAR [Marcinkevičs and Vogt(2021)], CUTS+ [Cheng et al.(2024)Cheng, Li, Xiao, Li, Suo, He, and Dai], JGC [Suryadi et al.(2023)Suryadi, Chew, and Ong], and JRNGC [Zhou et al.(2024)Zhou, Bai, Yu, Zhao, and Chen]. Additionally, the proposed model’s experimental hyperparameters are detailed in the Appendix. Our codes are provided in the supplementary material.

In alignment with prior studies, the model performances are evaluated using the area under the receiver operating characteristic curve (AUROC). Notably, in the evaluation of the gene regulatory networks, only the off-diagonal elements of the Granger causality adjacency matrix are considered since the gold standard provided by the gene regulatory networks does not account for self-causality. In contrast, for the Lorenz-96, fMRI BOLD, and VAR datasets, all elements of the adjacency matrix are included in the evaluation.

## 4.1 Lorenz-96

The Lorenz-96 model is a mathematical model employed to investigate the dynamics of simplified atmospheric systems. Its behavior is governed by the following ordinary differential equation:

$$\frac{\partial x_{t,i}}{\partial t} = -x_{t,i-1}(x_{t,i-2} - x_{t,i+1}) - x_{t,i} + F \quad (16)$$

Where  $F$  represents the external forcing term in the system, and  $p$  denotes the spatial dimension of the system. An increase in  $F$  results in heightened system chaos, while an increase in  $p$  enhances the spatial complexity of the system. We numerically simulate  $R = 5$  replicates under the following three conditions : (1)  $F = 10, P = 10, T = 1000$  (low dimensionality, weak nonlinearity); (2)  $F = 40, P = 40, T = 1000$  (high dimensionality, strong nonlinearity); (3)  $F = 40, P = 40, T = 500$  (limited observations).

Table 1: Performance on Lorenz-96 dataset.

Models	AUROC		
	$p = 10, F = 10$ $T = 1000$	$p = 40, F = 40$ $T = 1000$	$p = 40, F = 40$ $T = 500$
cMLP	0.983±0.003	0.867±0.025	0.843±0.036
cLSTM	0.978±0.004	0.943±0.027	0.863±0.044
TCDF	0.879±0.011	0.674±0.039	0.565±0.041
eSRU	<b>1.0±0.00</b>	0.973±0.012	0.953±0.025
GVAR	<b>1.0±0.00</b>	0.951±0.016	0.941±0.022
NAVAR (MLP)	0.993±0.004	0.843±0.033	0.787±0.054
NAVAR (LSTM)	0.993±0.006	0.821±0.045	0.791±0.056
JGC	0.994±0.005	0.944±0.037	0.927±0.053
CUTS+	<b>1.0±0.00</b>	0.989±0.003	0.963±0.012
JRNGC	<b>1.0±0.00</b>	0.979±0.012	0.956±0.023
<b>GCKAN</b>	<b>1.0±0.00</b>	<b>0.995±0.003</b>	<b>0.977±0.014</b>

Table 1 presents the Granger causality inference performance of each model under three conditions. For the scenario where  $p=10, F=10$ , and  $T=1000$ , all methods, except for TCDF, demonstrate the ability to infer causal relationships effectively. Notably, GCKAN, eSRU, GVAR, CUTS+, and JRNGC achieve an AUROC of 1.0. However, when  $F=40, P=40$ , causal inference becomes more challenging, particularly as the time series length decreases. Under these conditions, the performance of cMLP, cLSTM, and NAVAR declines significantly. GCKAN achieves the highest AUROC (0.995 and 0.977, respectively), though its advantage over CUTS+ and JRNGC is not significant. In summary, GCKAN exhibits superior performance on the Lorenz-96 dataset.

## 4.2 Gene regulatory networks

### 4.2.1 Dream-3

The second dataset is the DREAM-3 in Silico Network Challenge, available at <https://gnw.sourceforge.net/dreamchallenge.html>. This dataset provides a complex and nonlinear framework for evaluating the performance of Granger causality models. It consists of five sub-datasets: two corresponding to *E.coli* (*E.coli-1, E.coli-2*) and three to Yeast (*Yeast-1, Yeast-2, Yeast-3*). Each sub-dataset has a distinct ground-truth Granger causality network and includes  $p=100$  time series, which represents the expression levels of  $n=100$  genes. Each time series comprises 46 replicates, sampled at 21 time points, yielding a total of 966 observations.

The results of the Dream-3 dataset are shown in Table 2. The performance of all models drops significantly compared to the Lorenz-96 dataset since the Dream-3 dataset contains 100 channels, carries additional noise and has few observations, which leads to frequent overfitting of the models. Our model emerged as the top-performance model among its counterparts in four out of five gene regulatory networks. Specifically, the AUROC of the proposed model in *E.coli-1, E.coli-2, Yeast-1*, and *Yeast-3* are 0.762, 0.680, 0.667 and 0.562, respectively. Compared with the baseline, the performance is improved by 9.6%, 0.2%, 1.5% and 0.2%, respectively. This further proves the effectiveness of our method in identifying sparse Granger causality in high-dimensional, noisy time series.

### 4.2.2 Dream-4

The third dataset is the DREAM-4 in silico challenge. Analogous to the DREAM-3 dataset, it consists of five sub-datasets, each containing  $p = 100$  time series. However, unlike DREAM-3, each time series in DREAM-4 includes only 10 replicates sampled at 21 time points, yielding a total of 210 observations. This is substantially fewer than the 966 observations provided by the DREAM-3 dataset. Therefore, Dream-4 dataset challenges the inference performance of each model in scenarios with a limited number of time series observations.

Table 2: AUROC of the Dream-3 dataset, T=966, p=100

Models	AUROC				
	Ecoli-1	Ecoli-2	Yeast-1	Yeast-2	Yeast-3
cMLP	0.648	0.568	0.585	0.511	0.531
cLSTM	0.651	0.609	0.579	0.524	0.552
TCDF	0.615	0.621	0.581	0.567	0.565
eSRU	0.660	0.636	0.631	0.561	0.559
GVAR	0.652	0.634	0.623	0.57	0.554
NAVAR (MLP)	0.557	0.577	0.652	0.573	0.548
NAVAR (LSTM)	0.544	0.473	0.497	0.477	0.466
JGC	0.522	0.536	0.611	0.558	0.531
CUTS+	0.703	0.675	0.661	<b>0.612</b>	0.554
JRNGC	0.666	0.678	0.650	0.597	0.560
<b>GCKAN</b>	<b>0.762</b>	<b>0.680</b>	<b>0.667</b>	0.552	<b>0.562</b>

Table 3: AUROC of the Dream-4 dataset, T=210, p=100

Models	AUROC				
	Gene-1	Gene-2	Gene-3	Gene-4	Gene-5
cMLP	0.652	0.522	0.509	0.511	0.531
cLSTM	0.633	0.509	0.498	0.524	0.552
TCDF	0.598	0.491	0.467	0.567	0.565
eSRU	0.647	0.554	0.545	0.561	0.559
GVAR	0.662	0.569	0.565	0.578	0.554
NAVAR (MLP)	0.591	0.522	0.507	0.543	0.548
NAVAR (LSTM)	0.587	0.514	0.525	0.537	0.531
JGC	0.544	0.502	0.513	0.505	0.517
CUTS+	0.738	<b>0.622</b>	0.591	0.584	0.594
JRNGC	0.731	0.613	0.583	0.597	0.580
<b>GCKAN</b>	<b>0.747</b>	0.591	<b>0.602</b>	<b>0.613</b>	<b>0.601</b>

Table 3 shows the improved performance of the proposed GCKAN models in inferring gene-gene interactions from limited time-series data, outperforming baseline models. Specifically, GCKAN achieves the highest AUROCs in four of the five gene networks, with values of 0.747, 0.602, 0.613, and 0.601 for networks 1, 3, 4, and 5, respectively.

### 4.3 fMRI BOLD signals

The fourth dataset is the simulated fMRI BOLD signals generated using the dynamic causal model (DCM) with the nonlinear balloon model for vascular dynamics. Each data includes multiple time series corresponding to different brain regions of interest (ROIs). Notably, the fMRI BOLD dataset contains 28 sub-datasets, each comprising 50 subjects and including distinct features. However, previous studies have typically utilized few subjects from few simulations (e.g., sim-3, sim-4) for model evaluation, which is inadequate for comprehensively assessing model performance on the fMRI dataset. In this study, we address this limitation by conducting a thorough evaluation using the complete set of subject data from all simulations (a total of 1,400 subjects). The dataset is shared at <https://www.fmrib.ox.ac.uk/datasets/netstim/index.html>. Table 4 presents the comparison results of the first four simulations. The complete model performances and the summary of all the simulations' specifications are provided in the Appendix A Table 6, 7.

Comparative experiments conducted on the fMRI BOLD signal dataset demonstrate that only TCDF, JGC, JRNGC, CUTS+, and GCKAN effectively infer Granger causality across all simulations and subjects. Among these methods, GCKAN achieved superior performance in 22 out of 28 simulations, covering various complex scenarios such as global mean confusion, mixed time series, shared inputs, backward connections, cyclic connections, and time lags. In contrast, JRNGC and CUTS+ exhibited better performance in simulations with varying connection strengths (e.g., Sim 15, 22, 23). Furthermore, given the inclusion of noise and randomness (with a standard deviation of 0.5 seconds in the hemodynamic response function delay) and the limited sampling points (T=200) in most cases, the proposed model can more effectively infer Granger causality under noisy and data-constrained conditions compared to existing baseline models.



Table 4: AUROC of the fMRI BOLD signals, Subject=50

Models	AUROC			
	Sim-1	Sim-2	Sim-3	Sim-4
cMLP	0.746±0.04	0.733±0.05	0.705±0.06	0.685±0.06
cLSTM	0.689±0.05	0.739±0.04	0.735±0.05	0.711±0.05
TCDF	0.806±0.03	0.823±0.04	0.823±0.03	0.814±0.03
eSRU	0.729±0.04	0.756±0.04	0.737±0.04	0.722±0.04
GVAR	0.753±0.05	0.723±0.04	0.744±0.05	0.738±0.04
NAVAR (MLP)	0.723±0.04	0.701±0.03	0.703±0.03	0.688±0.04
NAVAR (LSTM)	0.711±0.05	0.694±0.03	0.679±0.04	0.647±0.05
JGC	0.812±0.05	0.842±0.02	0.866±0.02	0.854±0.02
CUTS+	0.825±0.04	0.851±0.03	0.859±0.02	0.869±0.02
JRNGC	<b>0.829±0.04</b>	0.833±0.02	0.831±0.03	0.877±0.01
<b>GCKAN</b>	0.815±0.08	<b>0.857±0.03</b>	<b>0.884±0.02</b>	<b>0.916±0.01</b>

## 4.4 VAR

### 4.4.1 experimental results

The fifth dataset is the VAR model. For a  $p$ -dimensional time series  $x_t$ , the VAR model is given by:

$$x_t = A^{(1)}x_{t-1} + A^{(2)}x_{t-2} + \dots + A^{(k)}x_{t-k} + u_t \quad (17)$$

where  $(A^{(1)}, A^{(2)}, \dots, A^{(k)})$  are regression coefficients matrices and  $u_t$  is a vector of errors with Gaussian distribution. We define *sparsity* as the percentage of non-zero coefficients in  $A^{(i)}$ , and different *sparsity* represent different quantities of Granger causality interaction in the VAR model. The comparison results of the VAR dataset are presented in Table 5.

Table 5: Performance on VAR dataset.

Models	AUROC		
	$p = 10, T = 1000$ <i>sparsity</i> = 0.2 <i>lag</i> = 3	$p = 10, T = 1000$ <i>sparsity</i> = 0.3 <i>lag</i> = 3	$p = 10, T = 1000$ <i>sparsity</i> = 0.2 <i>lag</i> = 5
cMLP	<b>1±0.00</b>	0.947±0.004	0.986±0.002
cLSTM	0.986±0.004	0.921±0.004	0.961±0.003
TCDF	0.879±0.011	0.759±0.007	0.823±0.006
eSRU	<b>1.0±0.00</b>	0.995±0.001	<b>1.0±0.00</b>
GVAR	<b>1.0±0.00</b>	0.992±0.002	<b>1.0±0.00</b>
NAVAR (MLP)	0.993±0.002	0.986±0.003	0.992±0.002
NAVAR (LSTM)	0.993±0.002	0.963±0.004	0.987±0.002
JGC	<b>1.0±0.00</b>	0.995±0.002	<b>1.0±0.00</b>
CUTS+	<b>1.0±0.00</b>	<b>1.0±0.00</b>	<b>1.0±0.00</b>
JRNGC	<b>1.0±0.00</b>	0.997±0.001	<b>1.0±0.00</b>
<b>GCKAN</b>	<b>1.0±0.00</b>	0.993±0.003	<b>1.0±0.00</b>

The comparison results reveal that all models, with the exception of TCDF, effectively infer Granger causality from the VAR dataset. Among these, CUTS+ demonstrates the highest performance, achieving an AUROC of 1.0 in three scenarios. GCKAN, JRNGC, JGC, GVAR, and e-SRU achieve an AUROC of 1.0 in two scenarios. For cMLP and cLSTM, the performance decreases slightly when lag or sparsity are varied.

## 5 Conclusion

In this study, we propose a novel neural network-based Granger causality model, termed Granger Causal Kolmogorov-Arnold Networks (GCKAN). The model leverages the base weights of the KAN layer, incorporating sparsity-inducing penalties and ridge regularization to infer the causal relationship. In addition, we develop an algorithm grounded

in time-reverse Granger causality to mitigate spurious connections and enhance inference performances. Extensive experiments validate that GCKAN can effectively infer interaction relationships in time series, outperforming the existing baselines. These results suggest that GCKAN brings a new avenue for advancing Granger causality inference. We anticipate that this model will inspire subsequent research to design more accurate and computationally efficient frameworks for Granger causality inference.

## References

- [Seth(2007)] Anil Seth. Granger causality. *Scholarpedia*, 2(7):1667, 2007.
- [Maziarz(2015)] Mariusz Maziarz. A review of the granger-causality fallacy. *The journal of philosophical economics: Reflections on economic and social issues*, 8(2):86–105, 2015.
- [Friston et al.(2014)] Karl J Friston, André M Bastos, Ashwini Oswald, Bernadette van Wijk, Craig Richter, and Vladimir Litvak. Granger causality revisited. *Neuroimage*, 101: 796–808, 2014.
- [Shojaie and Fox(2022)] Ali Shojaie and Emily B Fox. Granger causality: A review and recent advances. *Annual Review of Statistics and Its Application*, 9:289–319, 2022.
- [Bressler and Seth(2011)] Steven L Bressler and Anil K Seth. Wiener–granger causality: a well established methodology. *Neuroimage*, 58(2):323–329, 2011.
- [Barnett and Seth(2014)] Lionel Barnett and Anil K Seth. The mvgc multivariate granger causality toolbox: a new approach to granger-causal inference. *Journal of neuroscience methods*, 223:50–68, 2014.
- [Mele et al.(2022)] Marco Mele, Cosimo Magazzino, Nicolas Schneider, Antonia Rosa Gurrieri, and Hêriş Golpira. Innovation, income, and waste disposal operations in korea: Evidence from a spectral granger causality analysis and artificial neural networks experiments. *Economia Politica*, 39(2):427–459, 2022.
- [Chen et al.(2023)] Xiaowen Chen, Faustine Ginoux, Martin Carbo-Tano, Thierry Mora, Aleksandra M Walczak, and Claire Wyart. Granger causality analysis for calcium transients in neuronal networks, challenges and improvements. *Elife*, 12:e81279, 2023.
- [Ren et al.(2023)] Xiaohang Ren, Jingyao Li, Feng He, and Brian Lucey. Impact of climate policy uncertainty on traditional energy and green markets: Evidence from time-varying granger tests. *Renewable and Sustainable Energy Reviews*, 173:113058, 2023.
- [Tank et al.(2022)] Alex Tank, Ian Covert, Nicholas Foti, Ali Shojaie, and Emily B Fox. Neural granger causality. *IEEE Transactions on Pattern Analysis and Machine Intelligence*, 44(8):4267–4279, 2022.
- [Bussmann et al.(2021)] Bart Bussmann, Jannes Nys, and Steven Latré. Neural additive vector autoregression models for causal discovery in time series. In *Discovery Science: 24th International Conference, DS 2021, Halifax, NS, Canada, October 11–13, 2021, Proceedings 24*, pages 446–460. Springer, 2021.
- [Zhou et al.(2024)] Wanqi Zhou, Shuanghao Bai, Shujian Yu, Qibin Zhao, and Badong Chen. Jacobian regularizer-based neural granger causality. In *Forty-first International Conference on Machine Learning*, 2024.
- [Khanna and Tan(2019)] Saurabh Khanna and Vincent YF Tan. Economy statistical recurrent units for inferring nonlinear granger causality. *arXiv preprint arXiv:1911.09879*, 2019.
- [Nauta et al.(2019)] Meike Nauta, Doina Bucur, and Christin Seifert. Causal discovery with attention-based convolutional neural networks. *Machine Learning and Knowledge Extraction*, 1(1):19, 2019.
- [Cheng et al.(2024)] Yuxiao Cheng, Lianglong Li, Tingxiong Xiao, Zongren Li, Jinli Suo, Kunlun He, and Qionghai Dai. Cuts+: High-dimensional causal discovery from irregular time-series. In *Proceedings of the AAAI Conference on Artificial Intelligence*, volume 38, pages 11525–11533, 2024.
- [Liu et al.(2024)] Ziming Liu, Yixuan Wang, Sachin Vaidya, Fabian Ruehle, James Halverson, Marin Soljačić, Thomas Y Hou, and Max Tegmark. Kan: Kolmogorov-arnold networks. *arXiv preprint arXiv:2404.19756*, 2024.
- [Kiamari et al.(2024)] Mehrdad Kiamari, Mohammad Kiamari, and Bhaskar Krishnamachari. Gkan: Graph kolmogorov-arnold networks. *arXiv preprint arXiv:2406.06470*, 2024.
- [Hou and Zhang(2024)] Yuntian Hou and Di Zhang. A comprehensive survey on kolmogorov arnold networks (kan). *arXiv preprint arXiv:2407.11075*, 2024.
- [Cheng et al.(2023)] Yuxiao Cheng, Runzhao Yang, Tingxiong Xiao, Zongren Li, Jinli Suo, Kunlun He, and Qionghai Dai. Cuts: Neural causal discovery from irregular time-series data. *arXiv preprint arXiv:2302.07458*, 2023.
- [Marcinkevičs and Vogt(2021)] Ričards Marcinkevičs and Julia E Vogt. Interpretable models for granger causality using self-explaining neural networks. *arXiv preprint arXiv:2101.07600*, 2021.

- [Haufe et al.(2013)Haufe, Nikulin, Müller, and Nolte] Stefan Haufe, Vadim V Nikulin, Klaus-Robert Müller, and Guido Nolte. A critical assessment of connectivity measures for eeg data: a simulation study. *Neuroimage*, 64: 120–133, 2013.
- [van den Broek et al.(1998)van den Broek, Reinders, Donderwinkel, and Peters] Sebastianus Petrus van den Broek, F Reinders, M Donderwinkel, and MJ Peters. Volume conduction effects in eeg and meg. *Electroencephalography and clinical neurophysiology*, 106(6):522–534, 1998.
- [Nunez et al.(1997)Nunez, Srinivasan, Westdorp, Wijesinghe, Tucker, Silberstein, and Cadusch] Paul L Nunez, Ramesh Srinivasan, Andrew F Westdorp, Ranjith S Wijesinghe, Don M Tucker, Richard B Silberstein, and Peter J Cadusch. Eeg coherency: I: statistics, reference electrode, volume conduction, laplacians, cortical imaging, and interpretation at multiple scales. *Electroencephalography and clinical neurophysiology*, 103(5):499–515, 1997.
- [Winkler et al.(2016)Winkler, Panknin, Bartz, Müller, and Haufe] Irene Winkler, Danny Panknin, Daniel Bartz, Klaus-Robert Müller, and Stefan Haufe. Validity of time reversal for testing granger causality. *IEEE Transactions on Signal Processing*, 64(11):2746–2760, 2016.
- [Kořenek and Hlinka(2021)] Jakub Kořenek and Jaroslav Hlinka. Causality in reversed time series: Reversed or conserved? *Entropy*, 23(8):1067, 2021.
- [Pinkus(1999)] Allan Pinkus. Approximation theory of the mlp model in neural networks. *Acta numerica*, 8:143–195, 1999.
- [Schmidt-Hieber(2021)] Johannes Schmidt-Hieber. The kolmogorov–arnold representation theorem revisited. *Neural networks*, 137:119–126, 2021.
- [Suryadi et al.(2023)Suryadi, Chew, and Ong] Suryadi Suryadi, Lock Yue Chew, and Yew-Soon Ong. Granger causality using jacobian in neural networks. *Chaos: An Interdisciplinary Journal of Nonlinear Science*, 33(2), 2023.

## A The complete comparative results of the fMRI BOLD dataset

The results of each model on the fMRI BOLD dataset and the simulations' specification are shown in the Table 6, 7.

Table 6: AUROC of the FMRI BOLD signals, Subject=50

Dataset	AUROC										
	cMLP	cLSTM	TCDF	eSRU	GVAR	NAVAR (MLP)	NAVAR (LSTM)	JGC	CUTS+	JRNGC	GCKAN
Sim1	0.746±0.04	0.689±0.05	0.806±0.03	0.729±0.04	0.753±0.05	0.723±0.05	0.711±0.05	0.812±0.05	<u>0.825±0.04</u>	<b>0.829±0.04</b>	0.815±0.08
Sim2	0.733±0.05	0.739±0.04	0.823±0.04	0.756±0.04	0.723±0.04	0.701±0.03	0.694±0.03	0.842±0.02	<u>0.851±0.03</u>	0.833±0.03	<b>0.857±0.03</b>
Sim3	0.705±0.06	0.735±0.05	0.823±0.03	0.737±0.04	0.744±0.05	0.703±0.03	0.679±0.04	<u>0.866±0.02</u>	<u>0.859±0.02</u>	0.831±0.03	<b>0.884±0.02</b>
Sim4	0.685±0.06	0.711±0.05	0.814±0.03	0.722±0.04	0.738±0.04	0.688±0.04	0.647±0.05	0.854±0.02	<u>0.869±0.02</u>	<u>0.877±0.01</u>	<b>0.916±0.01</b>
Sim5	0.681±0.05	0.691±0.04	0.815±0.03	0.756±0.04	0.732±0.03	0.794±0.03	0.812±0.04	0.838±0.03	<u>0.849±0.04</u>	<u>0.851±0.05</u>	<b>0.861±0.05</b>
Sim6	0.723±0.15	0.738±0.09	0.811±0.02	0.751±0.03	0.775±0.03	0.826±0.03	0.842±0.03	0.881±0.03	<u>0.903±0.03</u>	0.891±0.03	<b>0.928±0.02</b>
Sim7	0.708±0.05	0.721±0.04	0.809±0.03	0.781±0.04	0.744±0.03	0.805±0.03	0.827±0.03	0.843±0.03	<u>0.866±0.05</u>	0.841±0.04	<b>0.902±0.04</b>
Sim8	0.549±0.15	0.522±0.09	0.661±0.08	0.605±0.09	0.644±0.07	0.601±0.12	0.572±0.11	0.629±0.09	0.684±0.08	<u>0.712±0.07</u>	<b>0.766±0.08</b>
Sim9	0.667±0.07	0.704±0.09	0.789±0.06	0.710±0.05	0.679±0.06	0.713±0.08	0.727±0.08	0.752±0.07	<u>0.819±0.06</u>	<u>0.806±0.06</u>	<b>0.830±0.08</b>
Sim10	0.632±0.07	0.648±0.09	0.749±0.06	0.677±0.11	0.688±0.08	0.709±0.11	0.736±0.12	0.675±0.08	<b>0.799±0.07</b>	<u>0.774±0.08</u>	<u>0.783±0.07</u>
Sim11	0.726±0.04	0.715±0.03	0.785±0.03	0.737±0.04	0.743±0.03	0.777±0.03	0.784±0.03	0.811±0.03	0.816±0.02	<u>0.829±0.03</u>	<b>0.837±0.03</b>
Sim12	0.738±0.05	0.751±0.03	0.803±0.04	0.755±0.03	0.734±0.04	0.796±0.03	0.782±0.03	0.802±0.05	0.817±0.04	<u>0.832±0.04</u>	<b>0.860±0.03</b>
Sim13	0.596±0.07	0.586±0.04	0.714±0.06	0.655±0.08	0.676±0.09	0.685±0.08	0.693±0.09	0.683±0.09	0.716±0.07	<u>0.739±0.07</u>	<b>0.757±0.08</b>
Sim14	0.617±0.08	0.654±0.07	0.722±0.06	0.689±0.07	0.673±0.09	0.716±0.08	0.724±0.07	0.741±0.06	0.759±0.07	<u>0.761±0.06</u>	<b>0.801±0.08</b>
Sim15	0.637±0.10	0.647±0.09	0.687±0.06	0.614±0.09	0.606±0.08	0.664±0.07	0.672±0.09	0.692±0.08	0.732±0.08	<b>0.773±0.09</b>	<u>0.745±0.08</u>
Sim16	0.604±0.11	0.618±0.13	0.706±0.08	0.653±0.09	0.635±0.09	0.623±0.07	0.646±0.09	0.638±0.12	<u>0.729±0.09</u>	0.713±0.11	<b>0.758±0.09</b>
Sim17	0.694±0.05	0.686±0.05	0.813±0.03	0.712±0.04	0.704±0.05	0.769±0.03	0.781±0.04	0.794±0.04	0.845±0.03	<u>0.862±0.04</u>	<b>0.894±0.03</b>
Sim18	0.657±0.07	0.660±0.07	0.778±0.03	0.684±0.05	0.691±0.06	0.725±0.06	0.748±0.05	0.751±0.06	<u>0.831±0.05</u>	<b>0.837±0.05</b>	0.818±0.06
Sim19	0.733±0.05	0.772±0.04	0.849±0.03	0.793±0.05	0.739±0.06	0.779±0.04	0.826±0.04	0.847±0.04	<u>0.871±0.03</u>	0.865±0.03	<b>0.906±0.03</b>
Sim20	0.750±0.04	0.795±0.09	0.861±0.02	0.822±0.03	0.765±0.05	0.819±0.03	0.853±0.04	0.877±0.02	<u>0.915±0.03</u>	0.898±0.02	<b>0.921±0.03</b>
Sim21	0.651±0.07	0.674±0.08	0.753±0.05	0.707±0.06	0.719±0.04	0.688±0.05	0.702±0.06	0.643±0.08	<u>0.786±0.06</u>	0.767±0.06	<b>0.812±0.07</b>
Sim22	0.674±0.06	0.682±0.06	0.746±0.05	0.718±0.07	0.726±0.05	0.649±0.07	0.674±0.06	0.661±0.07	0.797±0.05	<u>0.801±0.06</u>	<b>0.825±0.06</b>
Sim23	0.574±0.08	0.598±0.09	0.662±0.05	0.619±0.08	0.624±0.09	0.585±0.09	0.592±0.08	0.624±0.09	0.641±0.08	<b>0.705±0.09</b>	<u>0.671±0.08</u>
Sim24	0.526±0.09	0.547±0.13	0.570±0.06	0.558±0.06	0.561±0.08	0.529±0.11	0.548±0.12	0.534±0.07	<b>0.611±0.07</b>	0.581±0.07	<u>0.594±0.09</u>
Sim25	0.627±0.07	0.613±0.05	0.681±0.04	0.633±0.07	0.641±0.05	0.608±0.06	0.595±0.07	0.645±0.04	0.707±0.06	<u>0.728±0.06</u>	<b>0.763±0.08</b>
Sim26	0.593±0.07	0.588±0.07	0.668±0.07	0.612±0.06	0.633±0.07	0.590±0.06	0.563±0.06	0.634±0.05	0.682±0.08	<u>0.701±0.07</u>	<b>0.721±0.09</b>
Sim27	0.642±0.08	0.631±0.06	0.699±0.05	0.644±0.09	0.695±0.06	0.626±0.07	0.598±0.09	0.656±0.08	0.708±0.07	<u>0.727±0.06</u>	<b>0.753±0.08</b>
Sim28	0.688±0.06	0.658±0.05	0.762±0.04	0.709±0.06	0.735±0.05	0.641±0.04	0.603±0.04	0.743±0.07	0.764±0.08	<u>0.772±0.06</u>	<b>0.821±0.07</b>

Table 7: The simulations' specification of fMRI BOLD dataset

Dataset	Dimension	Time Samples	Noise	HRF std.dev. (s)	Other descriptions
Sim1	5	200	1%	0.5	
Sim2	10	200	1%	0.5	
Sim3	15	200	1%	0.5	
Sim4	50	200	1%	0.5	
Sim5	5	1200	1%	0.5	
Sim6	10	1200	1%	0.5	
Sim7	5	5000	1%	0.5	
Sim8	5	200	1%	0.5	Shared inputs
Sim9	5	5000	1%	0.5	Shared inputs
Sim10	5	200	1%	0.5	Global mean confound
Sim11	10	200	1%	0.5	Bad ROIs (Time series mixed with each other)
Sim12	10	200	1%	0.5	Bad ROIs (Mixed addition time series)
Sim13	5	200	1%	0.5	Existing backwards connections
Sim14	5	200	1%	0.5	Existing cyclic connections
Sim15	5	200	0.1%	0.5	Connection strength becomes stronger
Sim16	5	200	1%	0.5	Existing more connections
Sim17	10	200	0.1%	0.5	
Sim18	5	200	1%	-	
Sim19	5	2400	0.1%	0.5	Time lag=100ms
Sim20	5	2400	0.1%	-	Time lag=100ms
Sim21	5	200	1%	0.5	2-group test
Sim22	5	200	0.1%	0.5	Connection strength is non stationary
Sim23	5	200	0.1%	0.5	Connection strength is stationary
Sim24	5	200	0.1%	0.5	Only one strong external input
Sim25	5	100	1%	0.5	
Sim26	5	50	1%	0.5	
Sim27	5	50	0.1%	0.5	
Sim28	5	100	0.1%	0.5	